Calculating the width of an ultra-narrow resonance

S. A. Rakityansky[a,b], S. N. Ershov[a]

[a] Joint Institute for Nuclear Research, Dubna, Russia

[b] Department of Physics, University of Pretoria, Pretoria, South Africa

Keywords:

quantum resonances, Jost function, WKB, Gamow theory, nuclear decays

PACS numbers:

03.65.-w, 12.39.Pn, 23.50.+z, 23.60.+e, 25.85.-w, 21.10.Tg, 03.65.Sq, 03.75.Lm

February 10, 2024

Abstract

A reliable way of calculating the width, Γ, of an extremely narrow quantum resonance is suggested. The proposed method is based on expanding the Jost function in the Taylor series around the real resonance energy, E_r, and looking for its zero at the nearby complex point $E_r - i\Gamma/2$. The coefficients of such an expansion can be obtained by solving a set of coupled differential equations. Using two simple exactly solvable models, it is demonstrated that the method is efficient and accurate.

1 Introduction

As compared to the bound and scattering state problems in quantum mechanics, theoretical analysis of the resonant states always was and still remains much more difficult and even associated with some controversial interpretations such as, for example, the normalization of these states [1]. There are many different approaches to solving the resonant state problems (see, for example, Refs. [2, 3]). Among them the most accurate are those that are based on searching for the S-matrix poles at complex energies, $E = E_r - i\Gamma/2$, where E_r is the resonant collision energy and Γ is the width of the resonance. Most of these complex-energy methods

use the so-called complex scaling which is also called complex rotation of the coordinate (see Refs. [3–5]).

The complex-energy methods are not only accurate but also very efficient because they are able to produce both E_r and Γ at the same time. However, this their advantage turns into disadvantage when it comes to locating extremely narrow resonances. Any calculations with realistic forces can only be done numerically and with a finite accuracy. When searching for an S-matrix pole, one has to find the complex number $E = E_r - i\Gamma/2$ where both the real and imaginary parts are found within the same numerical uncertainty, ϵ, i.e. $E_r \pm \epsilon$ and $\Gamma \pm \epsilon$. The difficulty shows up when $\Gamma \ll E_r$. Indeed, if Γ is of the same (or smaller) order of magnitude as the numerical tolerance, ϵ, then Γ is lost, i.e. cannot be determined.

The need for analyzing extremely narrow resonances is not uncommon. For example, the halflife of the α-radioactive nucleus ^{238}U is 4.468×10^9 years [6], which corresponds to $\Gamma \sim 10^{-39}$ MeV, while the Q-value, i.e. the kinetic energy, E_r, of the α-particle that this resonant state emits is $E_r \approx 4.270$ MeV. It is doubtful that, within the complex-scaling approach and without additional effort or a trick, anybody could accurately locate the S-matrix pole that is so close to the real axis.

Usually, the problems like that are solved in a two-step approach, separating the determination of the real and imaginary parts of the complex energy. The idea behind such a separation is basically the same that was proposed by George Gamow many decades ago [7]. The real part of the energy, E_r, is found as the energy of the corresponding bound state under the assumption that the potential barrier, separating the internal and external regions of space, is impenetrable. Then the penetration of the barrier at the energy thus found is evaluated using the WKB approximation. Finally, the lifetime of the state (which is related to Γ) is deduced from E_r and the penetration probability. This final step is crucial and varies from one method to the other.

Originally, Gamow's theory was based on a simple intuitive picture of a particle moving to and fro between the barrier walls and colliding with them (attempting to escape) with the frequency determined by E_r. Nowadays, the approaches of this kind take into account the geometric shape of the nuclear state as well as the preformation probability of the emitted cluster. In a deformed nucleus the distances to the barrier are different in different directions.

In the present paper, we are developing a method for finding the complex resonance energy, $E = E_r - i\Gamma/2$, of an ultra-narrow resonance without using the WKB approximation and without resorting to the dubious notion of the barrier-assault frequency. Similarly to the Gamow theory, we find E_r and Γ separately, but we do it within a rigorous quantum mechanical approach.

At the first step the real part, E_0, of the energy is found (the same way as in Gamow's theory) assuming that the particle cannot escape. Actually, such an assumption does not generate any noticeable error because the penetration through the barrier for an ultra-narrow

resonance is significantly suppressed. After finding E_0, we consider the Taylor series expansion of the Jost function around this point (which is on the real axis) and determine a small complex number Δ such that the Jost function is zero (i.e. the S-matrix has a pole) at the energy $E_0 + \Delta$. Knowing Δ, we can find the width, $\Gamma = -2\mathrm{Im}(\Delta)$, as well as a small correction, $\mathrm{Re}(\Delta)$, to the resonance collision energy, i.e. $E_r = E_0 + \mathrm{Re}(\Delta)$.

Since the resonance is extremely narrow, the distance $|\Delta|$ between E_0 and the nearby complex resonance point is extremely small. This means that it is sufficient to keep only the constant and the linear terms in the Taylor expansion of the Jost function. For calculating the Taylor-series coefficients, we numerically solve a system of first-order differential equations with simple boundary conditions (see chapter 15 of the book [5]).

2 Neutral particles

To begin with and in order to present the main idea of the proposed method in a most simple and clear way, let us consider a system of two spinless and structureless particles interacting via a short-range central potential $U(r)$.

2.1 Direct search for the S-matrix poles

The radial Schrödinger equation describing the relative motion of these particles with the reduced mass μ and the reduced potential $V(r) = (2\mu/\hbar^2)U(r)$,

$$\left[\frac{d^2}{dr^2} + k^2 - \frac{\ell(\ell+1)}{r^2} - V(r)\right] u_\ell(E,r) = 0 \ , \tag{1}$$

where $k^2 = 2\mu E/\hbar^2$ is the wave number squared, can be transformed into the following equivalent system of the first-order differential equations (see chapter 2 of the book [5]):

$$\begin{aligned} \partial_r F_\ell^{(\mathrm{in})}(E,r) &= -\frac{h_\ell^{(+)}(kr)}{2ik} V(r) \left[h_\ell^{(-)}(kr) F_\ell^{(\mathrm{in})}(E,r) + h_\ell^{(+)}(kr) F_\ell^{(\mathrm{out})}(E,r)\right] \ , \\ \partial_r F_\ell^{(\mathrm{out})}(E,r) &= \frac{h_\ell^{(-)}(kr)}{2ik} V(r) \left[h_\ell^{(-)}(kr) F_\ell^{(\mathrm{in})}(E,r) + h_\ell^{(+)}(kr) F_\ell^{(\mathrm{out})}(E,r)\right] \ . \end{aligned} \tag{2}$$

In these equations, $h_\ell^{(\pm)}(z) = j_\ell(z) \pm i n_\ell(z)$ are the Riccati-Hankel functions defined as in Appendix D of the book [5]. In order to avoid possible confusion, it should be noted that we follow F. Calogero [8] who used the notation $j_\ell(z)$ and $n_\ell(z)$ for the Riccati-Bessel and Riccati-Neumann functions. The standard spherical Bessel and Neumann functions are therefore $j_\ell(z)/z$ and $n_\ell(z)/z$, respectively.

The unknown functions $F_\ell^{(\mathrm{in/out})}(E,r)$ are the factorized parts of the regular solution of (1),

$$u_\ell(E,r) = h_\ell^{(-)}(kr)F_\ell^{(\mathrm{in})}(E,r) + h_\ell^{(+)}(kr)F_\ell^{(\mathrm{out})}(E,r) \ . \tag{3}$$

The simple boundary conditions at $r=0$,

$$F_\ell^{(\mathrm{in})}(E,0) = F_\ell^{(\mathrm{out})}(E,0) = \frac{1}{2} \ , \tag{4}$$

make $u_\ell(E,r)$ behaving near the origin as the Riccati-Bessel function,

$$u_\ell(E,r) \underset{r\to 0}{\longrightarrow} j_\ell(kr) \ . \tag{5}$$

At large distances the functions $F_\ell^{(\mathrm{in/out})}(E,r)$ converge to the corresponding Jost functions,

$$f_\ell^{(\mathrm{in/out})}(E) = \lim_{r\to\infty} F_\ell^{(\mathrm{in/out})}(E,r) \ , \tag{6}$$

that determine the S-matrix,

$$S_\ell(E) = f_\ell^{(\mathrm{out})}(E)\left[f_\ell^{(\mathrm{in})}(E)\right]^{-1} \ . \tag{7}$$

Its poles can be found by looking for the roots of the equation

$$f_\ell^{(\mathrm{in})}(E) = 0 \ . \tag{8}$$

In searching for these roots, we numerically integrate Eqs. (2) for each complex value of E that is needed in the chosen search algorithm. The integration starts at $r=0$ with the boundary values (4) and stops at some faraway point $r_{\max}$ where the potential is practically zero (within the required accuracy) and where the limits (6) are therefore reached. As is explained in chapter 7 of the book [5], the integration of Eqs. (2) may require the complex rotation of the coordinate r, if the energy E is complex. In other words, to get to the point $r_{\max}$, we have to use a path (a detour) in the complex r-plane.

In Ref. [9] it was demonstrated that such an approach allows one to accurately locate very wide as well as very narrow resonances. However the uncertainty in determining Γ is the same as for the real part, E_r, of the resonance energy. This means that for $\Gamma \ll E_r$ (i.e. not for very narrow but for extremely narrow resonances) the method fails to determine Γ. A way to circumvent this difficulty is described next.

2.2 Power-series expansion of the Jost function

If Γ is extremely small, the search for the resonance root of Eq. (8) can be done in two steps. At the step one, we approximately determine the real part of the resonance energy, $E_0 \approx E_r$. To find E_0, we can look for the complex root as is described in the preceding section and temporarily ignore Γ (which is inaccurate anyway), or we can simply find the corresponding bound state energy under the assumption that the barrier is completely impenetrable. In fact, this means that the barrier at its highest value U_0 (see Fig. 1) extends to $r = \infty$ with a flat top. If the potential-well that is constructed in such a way near $r = 0$, supports a bound state, then E_0 is the (positive) energy of this state counted from the thereshold, $E = 0$, of the original problem. In the case of the simple potential depicted in Fig. 1, the potential well is formed by moving R_2 to infinity, and E_0 counted from the bottom of the well in the interval ①.

At the second step, we consider the Taylor expansion of the Jost function around the point E_0 (which is on the real axis),

$$f_\ell^{(\mathrm{in})}(E) = f_\ell^{(\mathrm{in})}(E_0) + \dot{f}_\ell^{(\mathrm{in})}(E_0)(E - E_0) + \frac{1}{2}\ddot{f}_\ell^{(\mathrm{in})}(E_0)(E - E_0)^2 + \dots \ , \tag{9}$$

where the "dot" means the derivative with respect to variable E. Since the resonance is extremely narrow, the point we are looking for is extremely close to E_0. This means that we can safely ignore all the higher powers of $(E - E_0)$ in (9) and retain only the constant and the linear terms,

$$f_\ell^{(\mathrm{in})}(E) = f_\ell^{(\mathrm{in})}(E_0) + \dot{f}_\ell^{(\mathrm{in})}(E_0)\Delta \ , \tag{10}$$

where $\Delta = E - E_0$. Therefore the complex root of Eq. (8) corresponds to

$$\Delta = -\frac{f_\ell^{(\mathrm{in})}(E_0)}{\dot{f}_\ell^{(\mathrm{in})}(E_0)} \ . \tag{11}$$

In other words, the complex number Δ added to the approximate real resonance energy, E_0, that was found at the first step, moves us from the real axis to the resonance pole. Therefore

$$\Gamma = -2\mathrm{Im}\,\Delta \tag{12}$$

and the value of $\mathrm{Re}\,\Delta$ gives the correction to the real part, namely, $E_r = E_0 + \mathrm{Re}\,\Delta$. Actually, if the resonance is extremely narrow, this correction is always beyond the required accuracy and can be ignored.

Therefore in order to find an extremely small Γ, we need not only the value of the Jost function, $f_\ell^{(\mathrm{in})}(E_0)$, but also its derivative, $\dot{f}_\ell^{(\mathrm{in})}(E_0)$, at the point E_0 on the real axis. The Jost

function can be easily calculated as is described in Sec. 2.1. What about its derivative? The direct numerical differentiation cannot be used if Γ is extremely small, because such a numerical procedure cannot give the necessary accuracy. In fact, the most efficient algorithm, the so called Newton method, for finding complex roots is based on such a numerical differentiation (see Ref. [10]). If it could provide a sufficient accuracy, we would simply locate the extremely narrow resonances the same way as is described in Sec. 2.1.

There is an alternative way of finding the Taylor-series coefficients in the expansion (9). It can be shown (see Sec. 7.7 of the book [5]) that in the case of a short-range single-channel potential the Jost functions have the following factorized structure:

$$f_\ell^{(\mathrm{in/out})}(E) = a_\ell(E) \mp ik^{2\ell+1} b_\ell(E) \ , \tag{13}$$

where the odd power of the momentum, $k^{2\ell+1}$, is the only factor responsible for the square-root branching of the Riemann surface. The unknown functions $a_\ell(E)$ and $b_\ell(E)$ are always single-valued and analytic.

Differentiating Eq. (13), we find:

$$\dot{f}_\ell^{(\mathrm{in})}(E) = \dot{a}_\ell(E) - i(2\ell+1)k^{2\ell}\dot{k} b_\ell(E) - ik^{2\ell+1}\dot{b}_\ell(E) \ , \tag{14}$$

where the derivative of k with respect to E is given by

$$\dot{k} = \frac{\mu}{\hbar^2 k} \ . \tag{15}$$

The fact that $a_\ell(E)$ and $b_\ell(E)$ are analytic allows us to expand them in the convergent Taylor series around the point E_0,

$$a_\ell(E) = \sum_{n=0}^{\infty} \alpha_n(\ell, E_0)(E-E_0)^n \ , \qquad b_\ell(E) = \sum_{n=0}^{\infty} \beta_n(\ell, E_0)(E-E_0)^n \ . \tag{16}$$

Actually, since we only need the first derivatives, $\dot{a}_\ell(E_0)$ and $\dot{b}_\ell(E_0)$, it is sufficient to find only the coefficients α_1 and β_1 of the linear terms in the expansions (16),

$$\dot{a}_\ell(E_0) = \alpha_1(\ell, E_0) \ , \qquad \dot{b}_\ell(E_0) = \beta_1(\ell, E_0) \ . \tag{17}$$

It can be shown (see Sec. 15.1.2 of the book [5]) that the coefficients α_n and β_n are the asymptotic values of the r-dependent functions $\tilde{\alpha}_n$ and $\tilde{\beta}_n$,

$$\alpha_n(\ell, E_0) = \frac{1}{2}\lim_{r\to\infty} \tilde{\alpha}_n(\ell, E_0, r) \qquad \beta_n(\ell, E_0) = \frac{1}{2}\lim_{r\to\infty} \tilde{\beta}_n(\ell, E_0, r) \ , \tag{18}$$

obeying the following set of differential equations:

$$\begin{aligned} \partial_r \tilde{\alpha}_n &= -\sum_{i+j+k=n} \gamma_i V(\varphi_j \tilde{\alpha}_k - \gamma_j \tilde{\beta}_k) \ , \\ \partial_r \tilde{\beta}_n &= -\sum_{i+j+k=n} \varphi_i V(\varphi_j \tilde{\alpha}_k - \gamma_j \tilde{\beta}_k) \ , \end{aligned} \tag{19}$$

with the boundary conditions

$$\tilde{\alpha}_n(\ell, E_0, 0) = \delta_{n0} \ , \qquad \tilde{\beta}_n(\ell, E_0, 0) = 0 \ , \qquad \forall\, n \ . \tag{20}$$

In Eqs. (19) the quantities φ_n and γ_n are the coefficients of the power-series expansions of the Riccati-Bessel and the Riccati-Neumann functions, $j_\ell(kr)$ and $n_\ell(kr)$, respectively. They can be found as follows (see Appendix D.2.1 of the book [5]):

$$\varphi_n(\ell, E_0, r) = \frac{1}{n!} \left[\left(-\frac{\mu r}{\hbar^2} \right)^n \frac{j_{\ell+n}(kr)}{k^{\ell+n+1}} \right]_{E=E_0} \ , \tag{21}$$

$$\gamma_n(\ell, E_0, r) = \frac{1}{n!} \left(\frac{\mu r}{\hbar^2} \right)^n \left[k^{\ell-n} n_{\ell-n}(kr) \right]_{E=E_0} \ . \tag{22}$$

The sums in Eqs. (19) only run over the subscripts obeying the condition $i+j+k=n$. This means that not all the equations in that system are coupled to each other. Since we need α_1 and β_1, it is sufficient to solve the first four equations,

$$\begin{aligned} \partial_r \tilde{\alpha}_0 &= -\gamma_0 V(\varphi_0 \tilde{\alpha}_0 - \gamma_0 \tilde{\beta}_0) \ , \\ \partial_r \tilde{\beta}_0 &= -\varphi_0 V(\varphi_0 \tilde{\alpha}_0 - \gamma_0 \tilde{\beta}_0) \ , \\ \partial_r \tilde{\alpha}_1 &= -\gamma_1 V(\varphi_0 \tilde{\alpha}_0 - \gamma_0 \tilde{\beta}_0) - \gamma_0 V(\varphi_1 \tilde{\alpha}_0 - \gamma_1 \tilde{\beta}_0) - \gamma_0 V(\varphi_0 \tilde{\alpha}_1 - \gamma_0 \tilde{\beta}_1) \ , \\ \partial_r \tilde{\beta}_1 &= -\varphi_1 V(\varphi_0 \tilde{\alpha}_0 - \gamma_0 \tilde{\beta}_0) - \varphi_0 V(\varphi_1 \tilde{\alpha}_0 - \gamma_1 \tilde{\beta}_0) - \varphi_0 V(\varphi_0 \tilde{\alpha}_1 - \gamma_0 \tilde{\beta}_1) \ . \end{aligned} \tag{23}$$

It is important to note that for real E_0 (central point of the Taylor expansion) all the coefficients in Eqs. (19) are real. This means that all α_n and β_n as well as a_ℓ and b_ℓ along the real axis are also real. Therefore $f_\ell^{(\mathrm{in})}(E_0) = \left[f_\ell^{(\mathrm{out})}(E_0) \right]^*$. The following fact needs to be emphasized: since E_0 is real, no complex rotation is needed when solving the system (23) (for more details see chapter 7 of the book [5]). This means that even a discontinuous or a tabulated potential can be used.

In summary, the procedure of finding an ultra-narrow resonance width is as follows:

- Firstly, we determine the real part of the resonance energy, $E_r \approx E_0$.
- Then we integrate the system (23) with the boundary values (20) from $r = 0$ up to a faraway point $r_{\max}$ where the potential on the right hand sides of Eqs. (23) vanishes and the limits (18) are reached.
- In this way, we obtain

$$\begin{aligned} f_\ell^{(\mathrm{in})}(E_0) &= \alpha_0 - ik_0^{2\ell+1}\beta_0 \ , \\ \dot{f}_\ell^{(\mathrm{in})}(E_0) &= \alpha_1 - i(2\ell+1)k_0^{2\ell}\dot{k}_0\beta_0 - ik_0^{2\ell+1}\beta_1 \ . \end{aligned}$$

- Finally, we find Δ and Γ as is given by Eqs. (11, 12).

2.3 Numerical example

In order to test the accuracy and efficiency of the proposed method, we consider a simple model potential for which the problem can be solved exactly. The chosen potential is shown in Fig. 1. This is a spherically symmetric square barrier,

$$U(r) = \begin{cases} 0 \quad , & 0 \leqslant r < R_1 \ , \\ U_0 \quad , & R_1 \leqslant r \leqslant R_2 \ , \\ 0 \quad , & r > R_2 \ . \end{cases} \tag{24}$$

It is clear that for this potential the collision energy, E_r, at which the lowest resonance occurs, should be close to the ground-state level in the square-well potential when $R_2 = \infty$. The greater is R_2, the closer E_r is to that bound-state level. At sufficiently large values of R_2 the point $E_0 \approx E_r$ (which is used for the Taylor expansion) is practically fixed (i.e. does not depend on R_2). By increasing R_2 further, we can arbitrarily reduce Γ of the resonance and thus can test the accuracy of our calculations at extremely small widths.

For the purpose of comparison, we need an exact solution of the problem. The regular solution of Eq. (1) with the potential (24) is known on each of the three intervals, ①, ②, and ③, where $U(r)$ is constant. The corresponding Jost function can be found in an explicit form via matching this regular solution at the points R_1 and R_2.

In order to avoid unnecessary complications, we consider the state with $\ell = 0$. In such a case the regular solution on the three intervals of r (shown in Fig. 1) looks as follows (we

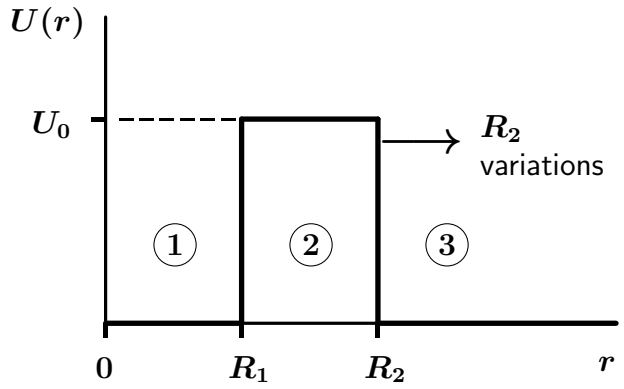

Figure 1: Square-barrier potential (24) that is used to test the accuracy of the method proposed in Sec. 2.2. At sufficiently large thickness of the barrier ② the resonant collision energy practically coincides with the bound state level of the square-well potential ① with $R_2 = \infty$. The width of this resonace can be arbitrarily decreased by moving R_2 to the right.

drop the subscript ℓ):

$$① \quad : \quad u(r) = \sin(kr) \ , \tag{25}$$

$$② \quad : \quad u(r) = xe^{ik_2 r} + ye^{-ik_2 r} \ , \tag{26}$$

$$③ \quad : \quad u(r) = ze^{ikr} + we^{-ikr} \ , \tag{27}$$

where

$$k_2 = \frac{1}{\hbar}\sqrt{2\mu(E - U_0)} = i\kappa \tag{28}$$

is (pure imaginary) local wave number on the interval ②, and x, y, z, w are some unknown constants determined by the smooth matching of the solutions (25, 26, 27) at the points R_1

and R_2. Equalizing the functions and their derivatives at these points, we obtain:

$$x = \frac{e^{-ik_2R_1}}{2ik_2}\left(ik_2\phi_1 + \phi_1'\right) \ , \tag{29}$$

$$y = \frac{e^{ik_2R_1}}{2ik_2}\left(ik_2\phi_1 - \phi_1'\right) \ , \tag{30}$$

$$z = \frac{e^{-ikR_2}}{2ik}\left(ik\phi_2 + \phi_2'\right) \ , \tag{31}$$

$$w = \frac{e^{ikR_2}}{2ik}\left(ik\phi_2 - \phi_2'\right) \ , \tag{32}$$

where

$$\phi_1 = u(R_1) = \sin(kR_1) \ , \tag{33}$$

$$\phi_1' = u'(R_1) = k\cos(kR_1) \ , \tag{34}$$

$$\phi_2 = u(R_2) = xe^{ik_2R_2} + ye^{-ik_2R_2} \ , \tag{35}$$

$$\phi_2' = u'(R_2) = ik_2\left(xe^{ik_2R_2} - ye^{-ik_2R_2}\right) \ . \tag{36}$$

The Jost functions are the amplitudes of the incoming and outgoing spherical waves in the asymptotic behaviour of the regular solution [5],

$$u_\ell(E,r) \underset{r\to\infty}{\longrightarrow} h_\ell^{(-)}(kr)f_\ell^{(\mathrm{in})}(E) + h_\ell^{(+)}(kr)f_\ell^{(\mathrm{out})}(E) \ . \tag{37}$$

Using the fact that $h_0^{(\pm)}(kr) = \mp ie^{\pm ikr}$, and comparing (37) with (27), we find that

$$f_0^{(\mathrm{in})} = -iw \ , \qquad f_0^{(\mathrm{out})} = iz \ . \tag{38}$$

Therefore the final explicit formula for $f_0^{(\mathrm{in})}$ can be obtained by sequential substitutions of Eqs. (29-36) into each other. It is simple but a bit cumbersome expression. We therefore do not write it here. Similarly, an explicit formula for the energy derivative of the Jost function, $\dot{f}_0^{(\mathrm{in})}$, can be obtained. This derivative is needed for finding the exact resonance-pole position, using Eqs. (10, 11, 12), when this pole is too close to the real axis. In such a case the Taylor expansion is necessary even if we have an explicit formula for $f_0^{(\mathrm{in})}$, because the root of Eq. (8) is found numerically anyway.

It is interesting to compare the ultra-narrow resonance widths obtained within our method, not only with their exact values but also with the corresponding values that are found within widely used Gamow theory. In this theory the probability, P, of penetration through a potential berrier between the classical turning points R_1 and R_2 is calculated using the WKB approximation (see, for example, chapter 6 of the book [12]),

$$P(E) = \exp\left\{-\frac{2}{\hbar}\int_{R_1}^{R_2} dr\sqrt{2\mu[U(r)-E]}\right\} \ . \tag{39}$$

In the case of our model potential the integral in this exponential function is trivial and we have

$$P(E_r) = \exp\left[-\frac{2}{\hbar}(R_2-R_1)\sqrt{2\mu(U_0-E_r)}\right] \ . \tag{40}$$

The frequency, ν, of assaulting the barrier is determined by the particle velocity, v, and the internal diameter, $2R_1$, which the particle needs to travel between any two collisions with the barrier,

$$\nu = \frac{v}{2R_1} = \frac{c}{R_1}\sqrt{\frac{E_r}{2\mu c^2}} \ . \tag{41}$$

The exponential constant, λ, in the radioactive-decay law, $N(t) = N(t_0)\exp(-\lambda t)$, is the product

$$\lambda = S\nu P \ , \tag{42}$$

where S is the probability of the emitted particle preformation. Since in the present paper we deal with a simple model where the emitted particle is always present, we put $S = 1$ and therefore

$$\Gamma = \hbar\lambda = \frac{\hbar c}{R_1}\sqrt{\frac{E_r}{2\mu c^2}}P(E_r) \ . \tag{43}$$

The parameters of our model potential (24) were chosen rather arbitrarily but when doing the choice we kept in mind the corresponding values that are typical in physics of heavy nuclei. The internal radius, R_1, was taken to be $6\,\mathrm{fm}$, which is roughly the radial size of the Uranium isotopes. The height of the barrier we used, $U_0 = 20\,\mathrm{MeV}$, is of the same order of magnitude as for many nuclear decay and fission processes. The reduced mass was (arbitrarily) taken to be equal to the mass of proton, $\mu = m_p$. With these parameters, the internal square-well potential (if we assume that $R_2 = \infty$) supports an S-wave bound state at the energy $4.11200126201\,\mathrm{MeV}$ above the bottom.

We started the calculations with $R_2 = 20\,\mathrm{fm}$ and gradually moved R_2 to the right. For each value of R_2, we calculated the parameters of the lowest resonance, E_r and Γ, using four different methods, namely,

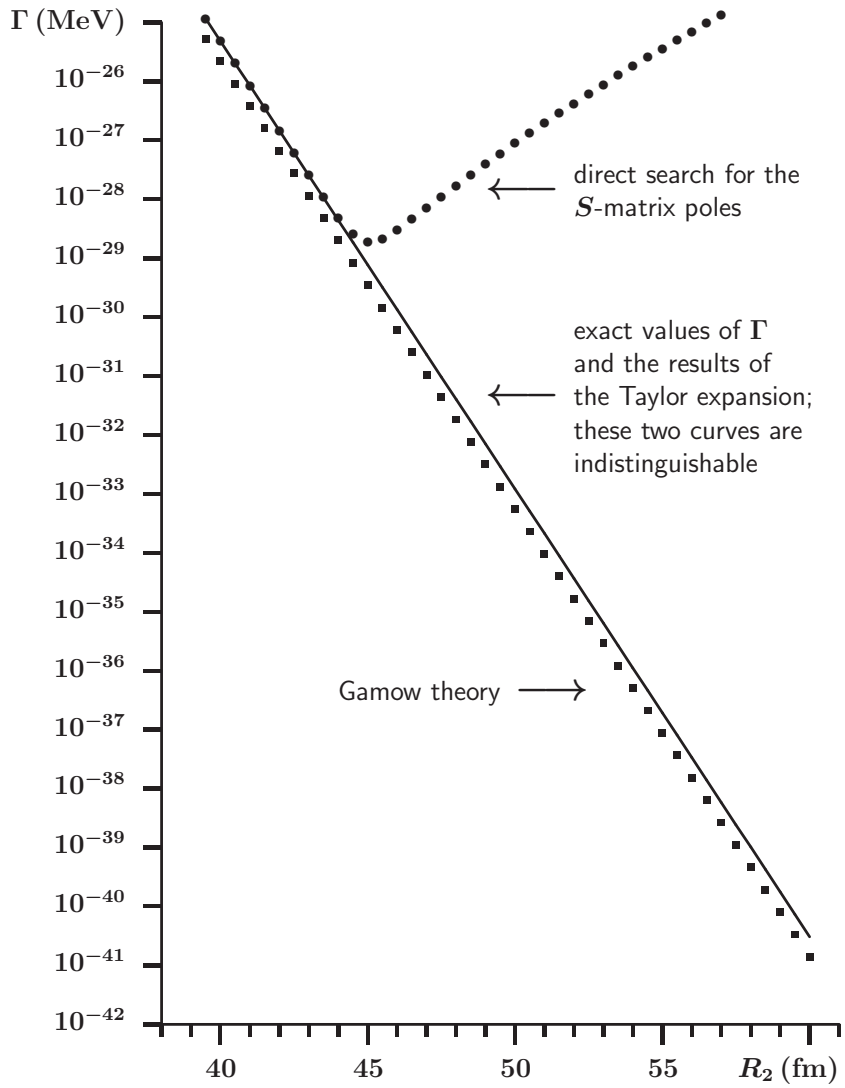

Figure 2: Variation of the width of the resonance generated by the square-barrier potential (shown in Fig. 1) when the barrier thickness increases. The continuous curve shows both the exact values of Γ and practically coinciding with them the points obtained with the help of the Taylor expansion. The round dots represent the results of the direct search for the Jost function zero at complex energies. The square dots are obtained using the standard Gamow theory.

1. Using the explicit formulae that detemine the Jost function (exact solution);

2. Using the Taylor expansion and integrating Eqs. (23);

3. Directly searching for the Jost function zero with the help of Eqs. (2);

4. Using Gamow formula (43).

The barrier for $R_2 = 20\,\mathrm{fm}$ is already sufficiently thick. The corresponding resonant energy, $E_r = 4.11200126198\,\mathrm{MeV}$ differs from the square-well bound state energy in the ninth digit after the decimal point. The resonance width was found to be $7.729561869 \times 10^{-11}\,\mathrm{MeV}$. These values of E_r and Γ turned out to be the same when we calculated them using the methods 1, 2, and 3. The Gamow method used at these R_2 and E_r gives $\Gamma = 3.521194750 \times 10^{-11}\,\mathrm{MeV}$, which differs from the exact value by the factor of ~ 2.2.

When increasing R_2, we found that the methods 1 and 2 always give the same results. The method 3 gives the correct Γ only up to $R_2 \sim 44\,\mathrm{fm}$. For larger values of R_2 (i.e. when $\Gamma \lesssim 10^{-29}\,\mathrm{MeV}$) the direct search of the S-matrix pole fails. The Gamow formula always gives a correct order of magnitude of Γ but its value remains smaller than the exact one by the same factor ~ 2.2. This is illustrated in Fig. 2.

Since the difference (by the factor of ~ 2.2) between the exact and Gamow values of Γ remains the same for different R_2, the reason for such an inaccuracy of the Gamow's theory can only be attributed to the simplified classical visualization of the decay process as a sequence of assaults of the barrier with the frequency ν given by Eq. (41). Although this is not the subject of the present paper, it is worthwhile to mention a couple of different approaches to calculating the frequency ν.

Some authors (see, for example, Refs. [13,14]) put the radius, R_1, instead of the diameter, $2R_1$, in the denominator of the first expression on the right hand side of Eq. (41). Possible explanation for such a choice could be found in considering quantum spherical wave that moves simultaneously in all directions and passes the distance R_1 before colliding with the barrier. Of course, this is also not a rigorous but a naive model consideration. However, it is a bit more "quantum" in contrast to the classical picture of a particle bouncing to and fro within the spherical shell. It is interesting to note that the frequency ν doubles as a result of such a "quantum" consideration. This would significantly reduce the difference between the exact and the Gamow curves in Fig. 2.

Yet another approach is based on using the relation $E = h\nu$ between the energy and the frequency, assuming that the assaults of the barrier result from quantum vibrations of the system (see, for example, Refs. [15, 16]). In some cases such a reasoning helps to increase Γ by a factor of ~ 2 as compared to the traditional model with bouncing particle.

As we already said, finding inaccuracy in the Gamow theory is not the subject but rather a byproduct of the present work. We only would like to note that, when doing an analysis of the decay processes, one should always keep in mind that this theory can only give the

correct order of magnitude of a resonance width. It may generate few times difference from the exact Γ. This fact should therefore be taken into account in estimating the ambiguity in the preformation factor S, when it is deduced from an experimental Γ with the help of Eq. (42).

3 Charged particles

Realistic physical systems that may exhibit the resonant behaviour with ultra-narrow widths, usually involve particles with electric charges. In the radial Schrödinger equation describing them, the total potential can always be split in a short-range part, $U(r)$, and pure Coulomb one,

$$\left[\partial_r^2 + k^2 - \frac{\ell(\ell+1)}{r^2} - V(r) - \frac{2k\eta}{r}\right] u_\ell(E,r) = 0 \ , \tag{44}$$

where $V = (2\mu/\hbar^2)U$ and $\eta = \mu e^2 Z_1 Z_2/(k\hbar^2)$ is the Sommerfeld parameter. The presence of the Coulomb potential makes significant changes to the theory described in the preceding sections (all the details can be found in Ref. [5]). In particular the Riccati-Hankel functions in Eqs. (2, 3) are replaced with the corresponding combinations, $H_\ell^{(\pm)}(\eta,kr) = F_\ell(\eta,kr) \mp iG_\ell(\eta,kr)$ of the standard regular and irregular Coulomb functions, F_ℓ and G_ℓ.

The main idea of finding an ultra-narrow Γ using Eqs. (11, 12), remains the same. However, the calculation of the numerator and denominator in Eq. (11) requires a bit more effort. First of all, the analytic structure of the Jost functions becomes more complicated as compared with Eq. (13) (see Eq. (8.100) of Ref. [5]):

$$f_\ell^{(\mathrm{in/out})}(E) = \frac{e^{\mp i\sigma_\ell}}{C_\ell(\eta)} \left\{ a_\ell(E) - \left[\frac{2\eta h(\eta)}{C_0^2(\eta)} \pm i\right] C_\ell^2(\eta) k^{2\ell+1} b_\ell(E) \right\} \ . \tag{45}$$

Similarly to (13) here the functions $a_\ell(E)$ and $b_\ell(E)$ are single-valued and analytic and therefore can be expanded in converging Taylor series. All the complications associated with multi-valuedness of the Jost functions and the branching of the Riemann surface where they are defined on, are caused by the explicitly given factors, where

$$\sigma_\ell(\eta) = \frac{1}{2i}\left[\ln\Gamma(\ell+1+i\eta) - \ln\Gamma(\ell+1-i\eta)\right] \underset{\eta\to 0}{\longrightarrow} 0 \ , \tag{46}$$

$$C_\ell(\eta) = \frac{e^{-\pi\eta/2}}{\Gamma(\ell+1)} \exp\left\{\frac{1}{2}\left[\ln\Gamma(\ell+1+i\eta) + \ln\Gamma(\ell+1-i\eta)\right]\right\} \underset{\eta\to 0}{\longrightarrow} 1 \ , \tag{47}$$

$$h(\eta) = \frac{1}{2}\left[\psi(i\eta) + \psi(-i\eta)\right] - \ln\eta \ , \qquad \psi(z) = \frac{\Gamma'(z)}{\Gamma(z)} \ . \tag{48}$$

As is seen, in order to find the derivative $\dot{f}_\ell^{(\mathrm{in})}$, we have to differentiate not only $a_\ell(E)$ and $b_\ell(E)$, but all the explicit factors as well. Such a differentiation gives:

$$\begin{aligned}\dot{f}_\ell^{(\mathrm{in})} &= -\left(\frac{\dot{C}_\ell}{C_\ell}+i\dot{\sigma}_\ell\right)f_\ell^{(\mathrm{in})}+\frac{e^{-i\sigma_\ell}}{C_\ell}\left\{\dot{a}_\ell-\left(\frac{2\eta h}{C_0^2}+i\right)C_\ell^2k^{2\ell+1}\dot{b}_\ell-\right.\\ &- (2\ell+1)k^{2\ell}\dot{k}C_\ell^2b_\ell\left[\left(\frac{2\eta h}{C_0^2}+i\right)\left(1+\frac{2}{2\ell+1}\frac{k\dot{C}_\ell}{\dot{k}C_\ell}\right)+\right.\\ &+ \left.\left.\frac{2}{2\ell+1}\frac{k}{\dot{k}\,C_0^2}\left(\dot{\eta}h+\eta\dot{h}-2\eta h\frac{\dot{C}_0}{C_0}\right)\right]\right\}\ . \qquad (49)\end{aligned}$$

It is not difficult to check that the derivatives of the explicitly known functions involved in this expression can be found as follows:

$$\dot{\eta} = -\eta\frac{\dot{k}}{k}\ , \qquad \dot{k}=\frac{\mu}{\hbar^2k}\ , \qquad (50)$$

$$\frac{\dot{C}_\ell}{C_\ell} = \frac{i}{2}\dot{\eta}\left[\psi(\ell+1+i\eta)-\psi(\ell+1-i\eta)+i\pi\right]\ , \qquad (51)$$

$$\frac{\dot{C}_\ell}{C_\ell}+i\dot{\sigma}_\ell = \dot{\eta}\left[i\psi(\ell+1+i\eta)-\frac{\pi}{2}\right]\ , \qquad (52)$$

$$\dot{h} = \frac{i}{2}\dot{\eta}\left[\psi'(i\eta)-\psi'(-i\eta)\right]+\frac{\dot{k}}{k}\ . \qquad (53)$$

The digamma function, ψ, is defined in (48), and its derivative can be found using Eqs. (6.3.5) and (6.4.1) of Ref. [11],

$$\psi'(z)=\psi'(z+1)+\frac{1}{z^2}\ , \qquad \psi'(z+1)=\int_0^\infty\frac{te^{-(z+1)t}}{1-e^{-t}}dt\ , \quad \mathrm{Re}\,(z+1)>0\ . \qquad (54)$$

Since in all our calculations the expansion point E_0 is on the real axis, the Sommerfeld parameter is also real. This means that $\psi(\ell+1+i\eta)=\psi^*(\ell+1-i\eta)$ and therefore

$$\psi(\ell+1+i\eta)-\psi(\ell+1-i\eta)=2i\,\mathrm{Im}\,\psi(\ell+1+i\eta)\ .$$

This imaginary part of the ψ-function can be found using Eqs. (6.3.5) and (6.3.11) of Ref. [11], namely,

$$\psi(z+1)=\psi(z)+\frac{1}{z}\ , \qquad \mathrm{Im}\,\psi(i\eta)=\frac{1}{2\eta}+\frac{\pi}{2}\coth(\pi\eta)\ .$$

The only quantities in Eq. (49) that remain unknown, are the derivatives $\dot{a}_\ell$ and $\dot{b}_\ell$. Similarly to the neutral-particle case (see Sec. 2.2), they can be found with the help of the Taylor expansions (16), where the coefficients α_n and β_n can be found using the same equations (18, 19, 20, 23), where the coefficients φ_n and γ_n are of course different (corresponding not to Riccati-Bessel and Riccati-Neumann but to the Coulomb functions). They can be calculated as is described in the Appendix A.

3.1 Numerical example

Similarly to Sec. 2.3, for the purpose of testing the theory, we choose here a simple square-well potential with a Coulomb tail extending to infinity (see Fig. 3),

$$U(r) = \begin{cases} U_0 & , \quad 0 \leqslant r < R \ , \\ \dfrac{e^2 Z_1 Z_2}{r} & , \qquad r > R \ . \end{cases} \tag{55}$$

In order to deal with the units typical for nuclear systems, the parameters of this potential were chosen in such a way that they are similar to those of the proton-emitting nucleus $^{19}\mathrm{Na}$. The inner radius R was taken to be $3\,\mathrm{fm}$ and the charges $Z_1 = 1$, $Z_2 = 10$. This makes the height of the Coulomb barrier at $r = R$ to be $\sim 4.8\,\mathrm{MeV}$. The depth of the inner potential well varies in our calculations from $-10\,\mathrm{MeV}$ to $-10.64\,\mathrm{MeV}$. With such a depth the lowest resonance is very close to the threshold ($16\,\mathrm{keV} \lesssim E_r \lesssim 400\,\mathrm{keV}$), where the Coulomb barrier is very thick and therefore Γ is very small. These values of U_0 of course do not correspond to actual depth of the $p^{18}\mathrm{Ne}$ interaction. Our calculations therefore cannot be considered as an attempt to describe this particular system. What we did was just an analysis of a model problem where the parameters where chosen to be similar to those for a real physical system. The reduced mass, μ, was also taken to be as for $p^{18}\mathrm{Ne}$.

To avoid unnecessary complications, we consider the S-wave case, $\ell = 0$. The Jost functions for such a problem can be found analytically (see Sec. 18.3 of the book [5]),

$$f_0^{(\mathrm{in/out})}(E) = \ \pm \ \frac{e^{\mp i\sigma_0(\eta)}}{2ik} \left[H_0^{(\pm)\prime}(\eta, kR)\sin(k_1 R) - H_0^{(\pm)}(\eta, kR) k_1 \cos(k_1 R) \right] \ , \tag{56}$$

where

$$k = \frac{1}{\hbar}\sqrt{2\mu E} \ , \qquad k_1 = \frac{1}{\hbar}\sqrt{2\mu(E - U_0)} \ , \qquad (U_0 < 0) \ , \tag{57}$$

and the "prime" means the derivative with respect to variable r.

The roots of this $f_0^{(\mathrm{in})}(E)$ on the uphysical sheet of the Riemann surface give us the exact resonance energies, $E_r - i\Gamma/2$. When doing numerical search for such roots, we should

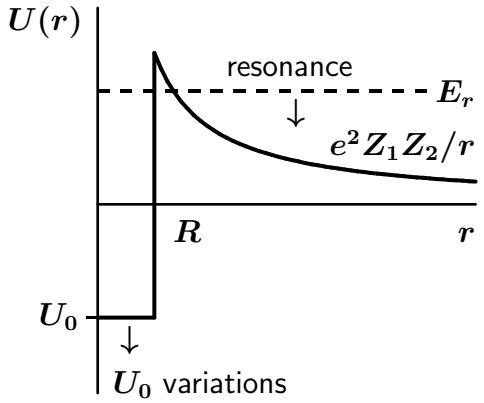

Figure 3: Square-well potential with the Coulomb tail for $r > R$, defined by Eq. (55). It is used to test the accuracy of the method proposed in Sec. 3. The collision energy, E_r, of a possible resonance for such a potential roughly corresponds to a bound-state level in the square-well with a completely impenetrable barrier. The width of this resonance can be arbitrarily decreased by moving U_0 down because such a change reduces E_r and thus makes the barrier more thick at the new level.

choose an appropriate sign in front of the square root (57) for k in order to make its imaginary part negative, which is equivalent to placing complex variable E on the unphysical sheet. The choice of the sign for k_1 is immaterial because it can only change the sign of the whole expression for $f_0^{(\mathrm{in})}(E)$ and thus does not play any role in Eq. (8).

When Γ becomes too small and we still try to find it via direct numerical search for the root of Eq. (8), the accuracy is lost (as is discussesd in Sec. 2.2) even if we use the exact formula (56) for the Jost function. This difficulty can be circumvented by using the first two terms of the Taylor series for the function $f_0^{(\mathrm{in})}(E)$ near the point E_r on the real axis. Its first derivative, $\dot{f}_0^{(\mathrm{in})}$, that is needed for that, can be found using Eq. (49). The functions $a_0(E)$ and $b_0(E)$ for the exact expression (56) are given by Eqs. (18.51, 18.52) of the book [5], namely,

$$a_0(E) = \frac{1}{2k}\left[\tilde{G}_0(E,R)k_1\cos(k_1R) - \tilde{G}_0'(E,R)\sin(k_1R)\right] , \tag{58}$$

$$b_0(E) = \frac{1}{2k}\left[\tilde{F}_0'(E,R)\sin(k_1R) - \tilde{F}_0(E,R)k_1\cos(k_1R)\right] , \tag{59}$$

where the tilded functions $\tilde{F}_0$ and $\tilde{G}_0$ are defined by Eqs. (67, 68) in Appendix A. The derivatives $\dot{a}_0$ and $\dot{b}_0$ can be evaluated via the corresponding derivatives of the functions $\tilde{F}_0$ and $\tilde{G}_0$ as is described in Appendix A. Some details of the numerical calculations are given in Appendix B.

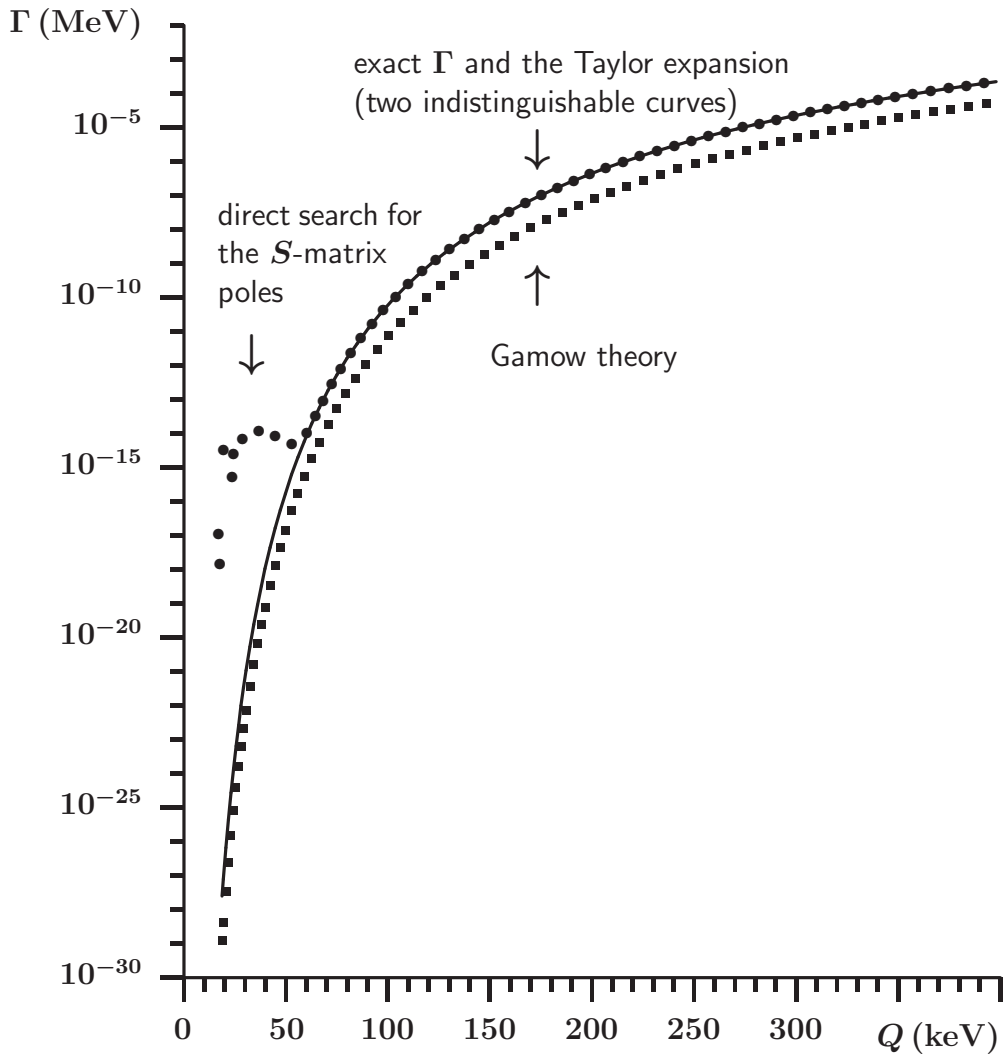

Figure 4: Dependence of the width of the lowest resonance generated by the potential shown in Fig. 3, on the Q-value which is equal to E_r, i.e. to the height of the resonance level above the threshold energy. The continuous curve shows both the exact values of Γ and practically coinciding with them the points obtained with the help of the Taylor expansion. The round dots represent the results of the direct search for the Jost function zero at complex energies. The square dots are obtained using the standard Gamow theory.

In a general case (when the Jost function is not known analytically), an ultra-narrow Γ can be found using the method, which we propose in the present work and which we are

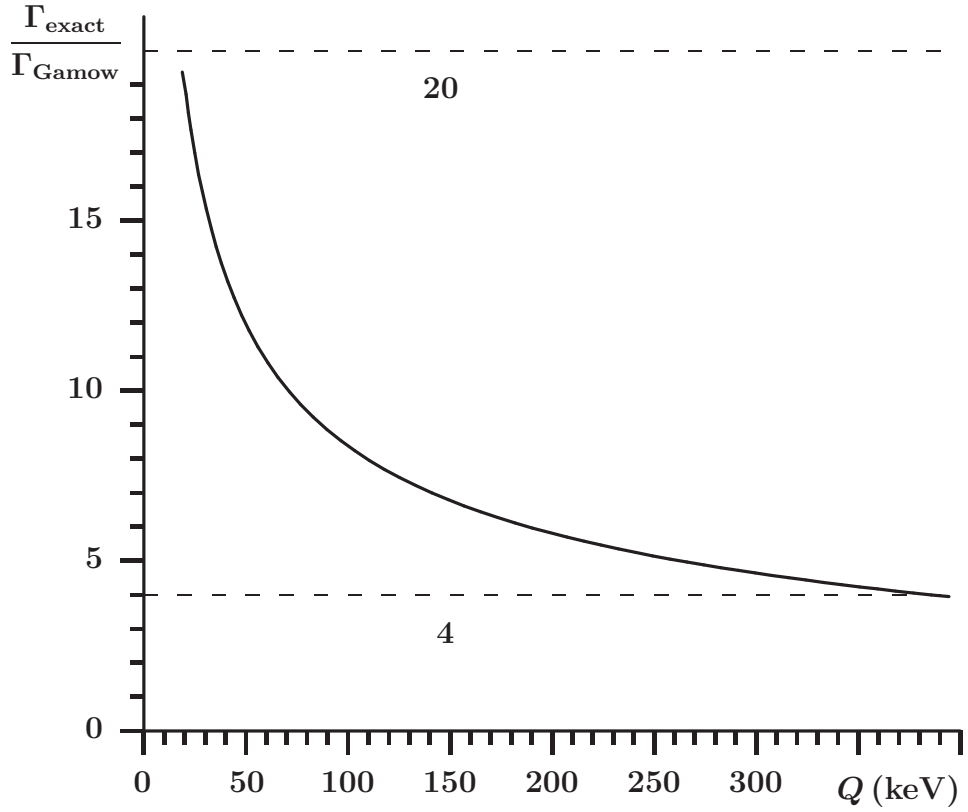

Figure 5: Ratio of the exact values of Γ to the corresponding widths obtained within the standard Gamow theory. This ratio is calculated for the curves shown in Fig. 4. The Q-value grows when the bottom of the square well potential (see Fig. 3) moves up. The horizontal dashed lines show the range within which the width ratio varies for the interval of the Q-values presented in the Figure.

testing in this numerical example. Within this method, we need to integrate the system of the differential equations (23). For the charged-particle case, the potential V in these equations is the short-range part of the total potential because the pure Coulomb term is present in Eq. (44) explicitly. In other words,

$$V(r) = \frac{2\mu}{\hbar^2} U(r) - \frac{2\eta k}{r} \ . \tag{60}$$

Therefore, in the numerical example we consider here, $V(r)$ is identical zero for $r > R$. In other words, this potential is of a finite range and therefore the integration of the differential equations (23) runs up to the point $r = R$, where the limits (18) are reached.

The results of our calculations for the potential (55) are shown in Fig. 4, where the notation and the symbols are the same as in Fig. 2. The difference is that here the width is given as the function of the Q-value of the decay, i.e. as the function of the height of the resonant energy above the threshold.

The exact values of Γ are presented in Fig. 4 by the solid curve. The corresponding values obtained with the help of the Taylor expansion, practically coincide with the exact ones and therefore lie on the same curve. The direct search for the Jost function zeros remains accurate for $\Gamma \gtrsim 10^{-14}\,\mathrm{MeV}$. For smaller widths this method gives completely wrong results (see round dots in Fig. 4).

Similarly to the neutral-particle case, the Gamow theory gives the widths that are systematically below the exact ones. It may seem that at small values of Γ the difference between the Gamow widths and the exact ones becomes smaller. This however is just an optical illusion because the scale on the vertical axis is logarithmic. The actual difference is shown in Fig. 5. As is seen, for extremely narrow resonances the Gamow theory may give even wrong order of magnitude of Γ.

4 Possible generalization for multi-channel problems

In multi-channel problems the Jost functions become matrices (see, for example, Chapter 12 of Ref. [5]). The S-matrix is their "matrix-ratio",

$$S(E) = f^{(\mathrm{out})}(E)\left[f^{(\mathrm{in})}(E)\right]^{-1} \ , \tag{61}$$

and the resonances correspond to zeros of the incoming Jost-matrix determinant on an appropriate sheet of the Riemann surface,

$$D(E) = \det f^{(\mathrm{in})}(E) = 0 \ . \tag{62}$$

If the resonance is extremely narrow, then the function $D(E)$ can be replaced with the first two terms of the Taylor series,

$$D(E) = D(E_0) + \dot{D}(E_0)\Delta \ , \tag{63}$$

where $\Delta = E - E_0$ is a complex number that determines the total width of the resonance as is given by Eq. (12), and E_0 is an approximately found resonant collision energy on the real axis. In order to find Δ, we need the values of the determinant and its energy-derivative at the point E_0,

$$\Delta = -\frac{D(E_0)}{\dot{D}(E_0)} \ . \tag{64}$$

The multi-channel Jost matrices (and therefore the determinant D) can be calculated using the matrix (and Coulomb) generalization of the differential equations (2) as is described in Ref. [5]. The derivative of the determinant is given by the trace of the following matrix product (see Eq. (F.13) of the book [5]):

$$\dot{D} = \mathrm{Sp}\left[M \cdot \dot{f}^{(\mathrm{in})}\right] \ , \tag{65}$$

where the square matrix M is composed of the transposed minors of the corresponding elements of $f^{(\mathrm{in})}$, such that

$$\left[f^{(\mathrm{in})}\right]^{-1} = \frac{M}{D} \ . \tag{66}$$

The derivatives, $\dot{f}^{(\mathrm{in})}$, of all the elements of the Jost matrix can be found either by a direct numerical differentiation, or (more accurately) in the way similar to the one described in the preceding sections for the single-channel case. Matrix generalizations of Eqs. (13) and (45) are given by Eqs. (13.24) and (14.70) of Ref. [5]. Chapter 15 of the same book describes the matrix versions of the Taylor expansions (16) as well as the corresponding differential equations that generalize Eqs. (19).

In addition to the total width given by Eq. (12), the partial widths for all the channels can be found as is described in Sec. (12.4.2) of Ref. [5].

Such a generalized multi-channel theory can be used, for example, to calculate the ultra-narrow widths of the two-body systems with non-central potentials, where each partial wave is a different channel with the same (degenerate) threshold energy. The theory can be further generalized to describe the N-body resonances using the expansion of the wave function over the hyperspherical harmonics. In doing this, we can introduce the N-body Jost matrices as is given in Sec. 17.1 of the book [5], and then can use the same multi-channel theory outlined here.

5 Conclusion

As is shown, the difficulties associated with calculation of the widths of extremely narrow resonances can be circumvented with the help of the Taylor series expansion of the Jost function. A way of finding the corresponding expansion coefficients is suggested. It is based on the semi-analytic representation (45) of the Jost function and on the differential equations (19) whose solutions asymptotically converge to the quantities that are part of the expression (49) for the first energy-derivative of the Jost function. Using two exactly solvable models, the accuracy of the suggested approach is demonstrated. Possible multi-channel generalization of the theory is discussed.

Appendices

A Power-series expansions of the Coulomb functions

The standard regular and irregular Coulomb functions, F_ℓ and G_ℓ, are multi-valued and are defined on a complicated Riemann surface (see, for example, Ref. [5]). Their analytic structure involves multi-valued as well as single-valued factors. The representations of F_ℓ and G_ℓ, where these factors are separated,

$$F_\ell(\eta, kr) = C_\ell(\eta) k^{\ell+1} \tilde{F}_\ell(E, r) \ , \tag{67}$$

$$G_\ell(\eta, kr) = \frac{2\eta h(\eta) C_\ell(\eta) k^{\ell+1}}{C_0^2(\eta)} \tilde{F}_\ell(\eta, kr) + \frac{1}{C_\ell(\eta) k^\ell} \tilde{G}_\ell(E, r) \ , \tag{68}$$

are used in Ref. [5] to derive the corresponding semi-analytic representations (45) of the Jost functions. In an explicit form the representations (67, 68) were obtained by J. Humblet in Ref. [17]. Here $\tilde{F}_\ell(E, r)$ and $\tilde{G}_\ell(E, r)$ are entire (analytic and single-valued) functions of the energy-variable E. They therefore can be expanded in converging Taylor series around an arbitrary complex point E_0,

$$\tilde{F}_\ell(E, r) = \sum_{n=0}^{\infty} \varphi_n(\ell, E_0, r)(E - E_0)^n \ , \tag{69}$$

$$\tilde{G}_\ell(E, r) = -\sum_{n=0}^{\infty} \gamma_n(\ell, E_0, r)(E - E_0)^n \ . \tag{70}$$

The expansion coefficients φ_n and γ_n are those that appear in the differential equations (19, 23) for the case of charged particles. The "minus" sign on the right hand side of Eq. (70) is chosen for the sake of keeping these differential equations in exactly the same form as for neutral particles. This is needed because the standard irregular Coulomb function is defined in such a way that $G_\ell \underset{\eta \to 0}{\longrightarrow} -n_\ell$. Then in the zero-charge limit the coefficients φ_n and γ_n that are defined here, should coinside with the corresponding coefficients given by Eqs. (21, 22).

In Ref. [17] Humblet derived explicit iterative formulae for calculating the coefficients φ_n and γ_n in the particular case $E_0 = 0$, i.e. for the Taylor expansions of the functions $\tilde{F}_\ell(E, r)$ and $\tilde{G}_\ell(E, r)$ around the threshold energy. Since these series are convergent on the whole plane of complex energies, we can use them to calculate the coefficients φ_n and γ_n for a pont $E_0 \neq 0$.

Below are the formulae extracted from Ref. [17]. It should be noted that our definition of the Coulomb barrier factor (47) differs from the one used by Humblet, by the factor of $1/(2\ell+1)!!$,

$$C_\ell^{\text{Humblet}} = \frac{1}{(2\ell+1)!!} C_\ell^{\text{our}} \ . \tag{71}$$

This is done to have the correct zero-charge limits in all the equations. It should also be noted that we give here the formulae for the case of a repulsive Coulomb potential and try to use the same notation (where possible) as in Ref. [17].

Using the appropriate equations from Ref. [17], we obtain the following:

$$\tilde{F}_\ell(E,r) = (2\ell)!!\, r^{\ell+1} \Phi_\ell(E,r) \ , \tag{72}$$

$$\Phi_\ell(E,r) = \sum_{m=0}^{\infty} (-1)^m \left(\frac{E}{g}\right)^m I_m^{(\ell)}(r) \ , \tag{73}$$

where

$$q = \frac{Z_1 Z_2 e^2 \mu}{\hbar^2} = \eta k \ , \qquad g = \frac{(\hbar q)^2}{2\mu} \ , \qquad x = \sqrt{8qr} \ , \tag{74}$$

$$I_m^{(\ell)}(r) = \frac{1}{12^m m!} \left(\frac{x}{2}\right)^{4m} \sum_{\lambda=0}^{m} a_{m\lambda}^{(\ell)} \left(\frac{x}{2}\right)^{-2\ell-1-m-\lambda} I_{2\ell+1+m+\lambda}(x) \ , \tag{75}$$

with $I_\ell(x)$ being the modified Bessel function of the first kind (see Ref. [11]). The coefficients $a_{m\lambda}^{(\ell)}$ can be found using the following recurrency relations:

$$a_{m\lambda}^{(\ell)} = 0 \qquad \text{for} \quad \lambda < 0 \ , \ \lambda > m \ , \tag{76}$$

$$a_{00}^{(\ell)} = 1 \ , \quad a_{10}^{(\ell)} = 1 \ , \quad a_{11}^{(\ell)} = \ell \ , \quad a_{m0}^{(\ell)} = 1 \ , \tag{77}$$

$$a_{mm}^{(\ell)} = \frac{\ell}{m} a_{m,m-1}^{(\ell)} \ , \quad m \geqslant 1 \ , \tag{78}$$

$$a_{m1}^{(\ell)} = m\left[\ell - \frac{1}{5}(m-1)\right] \ , \quad m \geqslant 1 \ , \tag{79}$$

$$a_{m2}^{(\ell)} = \frac{m(m-1)}{2}\left[\ell^2 - \frac{\ell}{5}(2m-3) + \frac{(m-2)(7m-1)}{175}\right] \ , \quad m \geqslant 2 \ , \tag{80}$$

$$\begin{aligned} a_{m3}^{(\ell)} \ &= \ \frac{m(m-1)(m-2)}{6}\left[\ell^3 - \frac{3\ell^2(m-2)}{5} + \right. \\ &+ \ \left. \frac{\ell(21m^2-66m+29)}{175} - \frac{(m-3)(m+1)(7m-10)}{875}\right] \ , \quad m \geqslant 3 \ , \end{aligned} \tag{81}$$

$$a^{(\ell)}_{m\lambda} = \frac{3m}{3m-\lambda} a^{(\ell)}_{m-1,\lambda} + \frac{(2\ell-m+\lambda)(m-\lambda+1)}{3m-\lambda} a^{(\ell)}_{m,\lambda-1} \ . \tag{82}$$

It is clear that for an arbitrary E_0

$$\begin{aligned} \varphi_n(\ell, E_0, r) &= \frac{1}{n!}\left[\partial^n_E \tilde{F}_\ell(E,r)\right]_{E=E_0} \qquad (83) \\ &= \frac{(2\ell)!!\, r^{\ell+1}}{g^n n!} \sum_{m=n}^{\infty} \frac{(-1)^m m!}{(m-n)!} \left(\frac{E_0}{g}\right)^{m-n} I^{(\ell)}_m(r) \ , \end{aligned}$$

which is the recipe for calculating φ_n that we were looking for.

Similarly, the coefficiets γ_n can be calculated. From the formulae derived in Ref. [17], we obtain (please take note of Eq. (71)):

$$\tilde{G}_\ell(E,r) = \left[\frac{C_\ell(\eta)}{C_0(\eta)}\right]^2 \sum_{m=0}^{\infty} (-1)^m \left(\frac{E}{g}\right)^{m+\ell} T^{(\ell)}_m(r) \ , \tag{84}$$

where

$$T^{(\ell)}_m(r) = -\frac{2(2\ell)!!\, q^{2\ell+1} r^{\ell+1}}{(2\ell+1)!!} \left[2K^{(\ell)}_m(r) + \sum_{s=0}^{m} (-1)^s b_s I^{(\ell)}_{m-s}(r)\right] \tag{85}$$

and $K^{(\ell)}_m(r)$ is a finite sum involving the modified Bessel functions of the second kind, $K_m(x)$ ($x = \sqrt{8qr}$),

$$K^{(\ell)}_m(r) = \frac{1}{12^m m!} \left(\frac{x}{2}\right)^{4m} \sum_{\lambda=0}^{m} a^{(\ell)}_{m\lambda} \left(-\frac{x}{2}\right)^{-2\ell-1-m-\lambda} K_{2\ell+1+m+\lambda}(x) \ . \tag{86}$$

The coefficients b_s in Eq. (85) are expressed via the Bernoulli numbers, B_n, with even subscripts,

$$b_0 = 0 \ , \qquad b_s = \frac{|B_{2s}|}{2s} \ , \quad s \geqslant 1 \ , \tag{87}$$

$$B_n = \lim_{t\to 0} \frac{d^n}{dt^n} \frac{t}{e^t - 1} \ . \tag{88}$$

From the definition (47) of the barrier factor and using the properties of the Γ-function, it is not difficult to find that

$$\left[\frac{C_\ell(\eta)}{C_0(\eta)}\right]^2 = \begin{cases} 1 & , \quad \ell = 0 \ , \\ \dfrac{1}{(\ell!)^2} \displaystyle\prod_{\lambda=1}^{\ell} (\lambda^2 + \eta^2) & , \quad \ell \geqslant 1 \ . \end{cases} \tag{89}$$

Therefore, since $\eta^2 = g/E$, the first energy-dependent factor in Eq. (84) is a polynomial of the ratio g/E and the highest power of this polynomial is ℓ. Taking the common factor $(E/g)^\ell$ out of the infinite series in that equation and introducing the polynomial

$$\begin{aligned}\mathcal{E}_\ell(E) &= \left(\frac{E}{g}\ell^2+1\right)\left[\frac{E}{g}(\ell-1)^2+1\right]\left[\frac{E}{g}(\ell-2)^2+1\right]\cdots\left(\frac{E}{g}+1\right)\\ &= \prod_{\lambda=0}^{\ell}\left(\frac{E}{g}\lambda^2+1\right)\ , \end{aligned} \tag{90}$$

we re-write Eq. (84) in the form

$$\tilde{G}_\ell(E,r) = \mathcal{E}_\ell(E)\sum_{m=0}^{\infty}(-1)^m\left(\frac{E}{g}\right)^m T_m^{(\ell)}(r)\ , \tag{91}$$

which is more convenient for calculating the E-derivatives that are needed for finding the coefficients γ_n:

$$\gamma_n(\ell,E_0,r) = -\frac{1}{n!}\left[\frac{d^n}{dE^n}\tilde{G}_\ell(E,r)\right]_{E=E_0}\ . \tag{92}$$

In fact, for our present calculations, we only need γ_0 and γ_1 (see Eq. (23)), which can be found as follows:

$$\gamma_0(\ell,E_0,r) = -\tilde{G}_\ell(E_0,r)\ , \tag{93}$$

$$\gamma_1(\ell,E_0,r) = -\sum_{m=0}^{\infty}(-1)^m\left(\frac{E_0}{g}\right)^{m-1}\left[\dot{\mathcal{E}}_\ell(E_0)\frac{E_0}{g}+\mathcal{E}_\ell(E_0)\frac{m}{g}\right]T_m^{(\ell)}(r)\ . \tag{94}$$

Using Eq. (90), we find that

$$\dot{\mathcal{E}}_\ell(E) = \sum_{\lambda'=0}^{\ell}\frac{\lambda'^2}{g}\prod_{\lambda=0,\lambda\neq\lambda'}^{\ell}\left(\frac{E}{g}\lambda^2+1\right)\ . \tag{95}$$

In the numerical calculations the sums $\sum_{m=0}^{\infty}$ in Eqs. (91) and (94) can usually be truncated at $m\sim 10$ depending on a required accuracy.

B Some details of the numerical calculations

All the numerical calculations presented in this paper, were done using the GNU-Fortran under Linux. For $\Gamma \gtrsim 10^{-14}\,\mathrm{MeV}$ it was sufficient to use the double precision, REAL*8 and

COMPLEX*16, for the real and complex variables, respectively. When the width becomes smaller, the necessary accuracy can only be achieved with the quadruple precision, REAL*16 and COMPLEX*32. It is not widely known and therefore should be mentioned that the transition from double to quadruple precision in the "gfortran" is simple and does not require revamping of the whole code. The compiler option "-freal-8-real-16" makes such a transition automatically.

For calculating the standard Coulomb functions $F_\ell(\eta, kr)$ and $G_\ell(\eta, kr)$, we used the fortran code "WCLBES" from the CERN library [18, 19].

The direct search for the Jost function zeros at complex energies was done using the Newton method in combination with the parabolic approximation of this function (see, Appendix H of the book [5]). When such a zero is close to the real axis a special care is needed in the algorithm for choosing the sign of the momentum k as well as in calculating the corresponding Coulomb-related functions (46, 47, 48). This is because at the real axis the unphysical sheet of the Riemann surface of the energy is connected to the physical sheet. When converging to the zero, the trial point E may jump above and below the real axis. This point must always be placed on the correct sheet.

Alternatively to the Newton method (which sometimes goes completely astray, if the starting point is chosen far from the zero we are looking for) we can locate the root of Eq. (8) as the minimum of the function $|f_\ell^{(\mathrm{in})}(E)|^2$. This method is less efficient because requires more calculations of the function, but it is more robust.

There is a useful numerical trick that can be very helpful when the root of Eq. (8) is too close to the real axis and therefore is difficult to locate. One of the parameters of the potential can be changed in such a way that this root is far enough from the axis. For instance, in the potential shown in Fig. 3, the inner potential well can be chosen shallow. After finding the root for this modified potential, we gradually (in small steps) move the modified parameter of the potential back to its actual value. In doing this, at each next step we choose the starting point for the Newton method as the root that was found at the previous step. If the steps are sufficiently small, then each new root is close to the previous one. This makes the searching algorithm stable.

References

[1] E. Brändas, N. Elander (Eds.), "Lecture Notes in Physics", vol. 325, "Resonances", Springer-Verlag: Berlin, Heidelberg: (1989)

[2] V. I. Kukulin, V. M. Krasnopol'sky, and J. Horàček, "Theory of Resonances: Principles and Applications", Kluwer Academic Publishers, Dordrecht/Boston/London (1989)

[3] Nimrod Moiseyev, "Non-Hermitian Quantum Mechanics", Cambridge University Press (2011)

[4] Nimrod Moiseyev, "Quantum theory of resonances: calculating energies, widths and cross-sections by complex scaling", Physics Reports, vol. 302, pp. 211-293 (1998)

[5] S. A. Rakitiansky, "Jost Functions in Quantum Mechanics: A Unified Approach to Scattering, Bound, and Resonant State Problems", Springer (2022)

[6] G. Audi, F.G. Kondev, Meng Wang, W.J. Huang, S. Naimi, "The N UBASE 2016 evaluation of nuclear properties", Chinese Physics C, Vol. 41, No. 3 (2017) 030001

[7] G. Gamow, "Zur Quantentheorie des Atomkernes", Z. Phys. $\mathbf{A51}$, pp. 204-212 (1928)

[8] F. Calogero, "Variable Phase Approach to Potential Scattering", Academic Press, New York (1967)

[9] S. A. Sofianos, S. A. Rakityansky, "Exact method for locating potential resonances and Regge trajectories", Journal of Physics, $\mathbf{A30}$, pp. 3725-3737 (1997)

[10] William H. Press, Saul A. Teukolsky, William T. Vetterling, Brian P. Flannery, "Numerical Recipes in Fortran 77: The Art of Scientific Computing", Second Edition, Press Syndicate of the University of Cambridge: New York (1997)

[11] M. Abramowitz and I. A. Stegun, "Handbook of Mathematical Functions", Dover Publications, Inc., New York (1972)

[12] W. S. C. Williams, "Nuclear and Particle Physics", Oxford University Press (1991)

[13] Carlos A. Bertulani, "Nuclear Physics in a Nutshel", Chapter 7, Princeton University Press, (2007)

[14] R. J. Liotta, "Developments in radioactive decay during the last Century", Journal of Physics: Conference Series, Vol. 413, 012012 (2013)

[15] H. F. Zhang, G. Royer, J. Q. Li, "Assault frequency and preformation probability of the α-emission process", Phys. Rev., $\mathbf{C\ 84}$, 027303 (2011)

[16] Qiong Xiao, Jun-Hao Cheng, Tong-Pu Yu, "Half-lives for proton emission and α decay within the deformed Gamow-like model", https://doi.org/10.48550/arXiv.2212.02898 (2022)

[17] J. Humblet, "Analytic Structure and Properties of Coulomb Wave Functions for Real and Complex Energies", Annals of Physics, Vol. 155, pp. 461-493 (1984)

[18] https://cernlib.web.cern.ch/download/2006_source/tar/ (2006)

[19] I.J. Thompson and A.R. Barnett, "Coulomb and Bessel Functions of Complex Arguments and Order", J.Comp.Phys., Vol. 64, pp. 490-509 (1986)